Nanoscale

PAPER

View Article Online
View Journal | View Issue

Cite this: *Nanoscale*, 2026, **18**, 5544

Room temperature sonochemically-initiated dehydrogenative coupling of silanes on silicon nanoparticle surfaces

Jonathan Trach, [a] Cole Butler,[a] Mia Dolanjski,[a] Alkiviathes Meldrum [b] and Jonathan G. C. Veinot *[a]

Received 11th November 2025,
Accepted 10th February 2026

DOI: 10.1039/d5nr04768d

rsc.li/nanoscale

Dehydrogenative coupling provides a convenient approach for forming Si–Si bonds in molecular systems and on silicon surfaces. Most procedures require the use of transition metal catalysts, which can limit adoption due to cost and contamination – this is particularly true when considering silicon nanoparticles (SiNPs). We demonstrate a catalyst-free method that uses an ultrasonication bath and a radical initiator to drive the dehydrocoupling reaction forward at room temperature to functionalize SiNP surfaces. This approach is tolerant of all types of silanes tested, including primary alkyl and aryl, secondary, and tertiary silanes, and provides comparable reactivity to standard catalyzed systems (*i.e.*, surface coverages of ~10%) while maintaining SiNP photoluminescence response. To our surprise, this new functionalization approach is the first reported approach that provides controlled synthesis of amorphous SiNPs.

Introduction

Silicon is the workhorse material for the electronics industry and its unique nanoscale properties continue to draw substantial attention.[1,2] The tunable photoluminescence and biocompatibility of silicon nanoparticles (SiNPs) have enabled many prototype applications including bioimaging,[3–5] energy storage,[6–8] drug delivery,[9–11] and flexible electronics.[12–14] However, SiNP properties can be compromised if exposed to ambient conditions.[15] The most common approaches for circumventing this is protecting their surfaces *via* passivation/functionalization. Doing so renders silicon surfaces resistant to the ambient environment and, depending upon the surface moieties, imparts solvent compatibility and reactivity, and strongly affects the luminescence.[16–19]

The most commonly applied methodology for tailoring Si surface chemistry exploits the hydrosilylation reaction that formally adds a Si–H bond across a multiple bond (*e.g.*, carbon–carbon double and triple bonds, C=O bonds in ketones and aldehydes, *etc.*).[20] Hydrosilylation reactions can be initiated photochemically, thermally, sonochemically, with radical sources, or catalytically.[21–28] In order to expand the substrate scope beyond Si–C bonds, and enable other reactivity, it is useful to consider reaction types such as dehydrogenative coupling.

Molecular dehydrogenative coupling has been studied for more than a century.[29,30] Silicon–silicon bond formation involves the formal cleavage of two Si–H bonds and the formation of a Si–Si bond with the corresponding release of H_2. It is well-established that this reaction is influenced by the degree of substitution at the silicon center and that an increased number of substituents decreases reactivity.[31–36] Dehydrogenative coupling has also been extended to Si surface chemistry.[37–39] Silicon wafers have been functionalized with primary alkyl silanes under thermally-activated conditions (*i.e.*, 80 °C).[39] Porous silicon surfaces were also modified with primary silanes using a zirconocene catalyzed reaction.[37] Under these conditions, aryl silanes were found to be the most reactive while surface grafting of aliphatic silanes was also possible. We also used Wilkinson's catalyst to facilitate dehydrogenative coupling on silicon nanoparticle (SiNP) surfaces, however the luminescence of the SiNPs was compromised by trace metal impurities.[38] Realizing a metal-free method to promote dehydrogenative coupling on SiNP surfaces while preserving material optical properties is clearly an attractive target that offers increased surface chemistry versatility, particularly if the substrate scope can be expanded (*e.g.* to secondary and tertiary silanes, which do not exhibit reactivity with current methods) without compromising reactivity.

Ultrasonication has emerged as a convenient, room temperature method for initiating hydrosilylation on SiNP surfaces that has the potential to activate dehydrogenative coupling without metal-based catalysts. It creates acoustic cavitation bubbles that produces localized areas of extreme temperature

[a]*University of Alberta, 11227 Saskatchewan Drive, Edmonton, Alberta T6G 2G2, Canada. E-mail: jveinot@ualberta.ca*
[b]*Department of Physics, University of Alberta, Edmonton, AB T6G 2E1, Canada*

and pressure (*i.e.*, 5000 K and 1000 bar).[40–42] Herein, we present our investigations into room temperature sonochemical-initiated dehydrogenative coupling of silanes on SiNP surfaces.

Materials

Sulfuric acid (reagent grade, 95–98%) was purchased from Caledon Laboratory Chemicals. Hydrofluoric acid (HF; electronics grade, 48–50%) was purchased from Fisher Scientific. Dodecylsilane (>95%), diisopropylsilane (>95%), and trioctylsilane (>95%) were purchased from Gelest. Fuming sulfuric acid (reagent grade, 20% free SO_3 bases), trichlorosilane (99%), toluene (HPLC grade), methanol (reagent grade), ethanol (100%, reagent grade), 2,2′-azobis(2-methyl propionitrile) (98%), 1-dodecene (95.0), and benzene (anhydrous, 99.8%) were purchased from Sigma Aldrich. A PureSolv purification system (Innovative Technology, Inc.) equipped with N_2 as the operating gas was used to prepare dry toluene. Air- and water-free reagents (1-dodecene, methanol) were prepared *via* three freeze–pump–thaw cycles and addition of activated molecular sieves. All reagents and solvents were used as received unless otherwise specified.

Preparation of hydrogen silsesquioxane

Hydrogen Silsesquioxane (HSQ) was synthesized using a modified literature procedure.[43] Briefly, a mixture of concentrated (70 mL) and fuming sulfuric acid (32.5 mL) was prepared in a three-neck round bottom flask purged with argon and equipped with an addition funnel and a Teflon coated stir bar. Dry toluene (210 mL) was then added to the acids *via* the addition funnel to obtain two layers. A mixture of dry toluene (510 mL) and trichlorosilane (75 mL) was prepared and subsequently added dropwise into the acid-toluene mixture. The toluene layer was isolated and washed with an aqueous sulfuric acid (33% v/v) solution. The organic layer was then dried over solid $MgSO_4$ and $CaCO_3$ for 12 h, followed by centrifugation at 11 000 RPM (12 739*g*) and suction filtration to remove the excess solid. Finally, the solvent was removed using rotary evaporation and dried *in vacuo* to yield *ca.* 20 g of a white solid (66% yield). The HSQ was stored under vacuum in the dark until use.

Preparation of SiNP/SiO_2 composite

SiNPs were prepared *via* thermal disproportionation of HSQ, using well-established procedures developed in our laboratory.[43] HSQ (*ca.* 3 g) was heated in an yttria stabilized zirconia boat (Almath Crucibles, Ltd) inside of a standard laboratory tube furnace (SentroTech, STT-1600C) to 1100, 1200, or 1300 °C under Ar flow to yield a SiNP/SiO_2 composite comprising a silica matrix containing *ca.* 3, 6, and 9 nm Si(0) inclusions, respectively. The composite was then mechanically ground using an agate mortar and pestle followed by shaking with glass beads in *ca.* 300 mL of absolute ethanol using a standard wrist action shaker for 12 h. Filtering and drying quantitively provided a fine brown powder.

Preparation of hydride-terminated Si nanoparticles

The SiNP/SiO_2 composite (*ca.* 500 mg) was dispersed in a 1 : 1 : 1 mixture of ethanol : distilled water : 48% hydrofluoric acid (total volume 15 mL) in a PET beaker and stirred using a Teflon coated stir bar for *ca.* 1 h. Toluene (*ca.* mL) was added to the etching mixture to recover the hydrophobic hydride terminated silicon nanoparticles (H-SiNPs). The toluene layer was decanted and the extract was subsequently centrifuged at 3500 RPM (1300*g*), the clear colourless toluene layer was decanted, and the orange pellet was washed twice more with fresh toluene (2 × 5 mL) and recovered each time upon centrifugation. These H-SiNPs were used immediately in functionalization reactions (see below) after purification.

Sonochemical dehydrocoupling procedure

In a typical reaction, a standard microwave reactor vial (Biotage Product 354 833) was loaded with dry toluene (*ca.* 4 mL) and the silane of choice (*ca.* 0.2 mL) and sealed with a septum cap (Biotage Product 352298) inside of an Ar filled glovebox. The sealed vial was removed from the glovebox and a suspension of H-SiNPs (*ca.* 25 mg) in dry toluene (1 mL) was added *via* syringe transfer. Subsequently, a radical initiator of choice (*i.e.*, 100 mg of 2,2′-azobis(2-methyl propionitrile) (AIBN) or 150 mg of benzoyl peroxide,) was dissolved in 1 mL of dry toluene and transferred to the reaction vial *via* syringe. The vial was then placed in a standard ultrasonic bath (Fisher Scientific, FS125) at 42 kHz for 24 h. A water circulation system (Thermo Scientific, Neslab RTE 7) was used to maintain the water level and bath temperature at 25 °C throughout the reaction. The sealed reaction vial was then removed from the sonication bath and the contents directly transferred to a centrifuge tube. Methanol (*ca.* 5 mL) was added to the centrifuge tube to induce precipitation of the functionalized SiNPs and the resulting solid product was isolated *via* centrifugation a 11 000 RPM (12 739*g*) for 20 minutes. The functionalized SiNPs were then redispersed in dry toluene (*ca.* 1 mL) without sonication and then methanol (*ca.* 5 mL) was added to induce precipitation. The precipitate was then isolated *via* centrifugation at 11 000 RPM (12 739*g*) for 20 minutes. This dispersion/centrifugation procedure was repeated twice. The purified functionalized particles (*ca.* 25 mg) were then dispersed without sonication in a minimum amount of benzene (*ca.* 1 mL) and freeze-dried before being characterized by FT-IR, TGA, XPS, and STEM.

Fourier-transform infrared spectroscopy

Samples of hydrogen-terminated and functionalized SiNPs for FT-IR analyses were prepared by drop casting from dry toluene suspensions onto silicon wafers. The solvent was evaporated, and spectra were then acquired using a Thermo Nicolet 8700 FT-IR Spectrometer equipped with a microscope.

Thermogravimetric analysis

Thermogravimetric analysis was obtained using a PerkinElmer Pyris 1 system in a flowing Ar atmosphere. Samples were prepared by loading functionalized SiNPs (*ca.* 2–5 mg) into a platinum pan and heating over a range of 20–700 °C, at a rate of 10 °C min^{-1}. Surface coverage was estimated from TGA mass loss data as described in the SI.

X-Ray powder diffraction

Powder samples were placed on a zero-background Si(100) wafer and analyzed in a Bruker D8 Advance powder diffractometer, using a SSD160 detector and a Cu radiation source ($K_{\alpha 1}$ = 1.54056 Å), operating at 40 kV and 40 mA.

X-Ray photoelectron spectroscopy

X-ray photoelectron spectroscopy (XPS) was performed using a Kratos Axis 165 Ultra X-ray photoelectron spectrometer equipped with a monochromatic Al Kα radiation source (1486.6 eV) operating at 210 W. High-resolution spectra were measured using an analyzer pass energy of 20 eV and a step of 0.1 eV. For survey spectra, a pass energy of 160 eV and a step of 0.5 eV were used. Spectra were calibrated to C 1s 284.8 eV using adventitious carbon. Sample preparation involved adhering solid SiNPs to carbon tape on a metal loading bar. Samples were analyzed and fit using CasaXPS, utilizing a Shirley-type background. The Si 2p region was fit using established values for the Si $2p_{1/2}$ and Si $2p_{3/2}$ spin–orbit coupling of 0.63 eV, with doublet area ratios fixed at 1 : 2 and full-width at half-maximum ratios fixed at 1 : 1.

Scanning/transmission electron microscopy

Scanning/transmission electron microscopy (S/TEM) images were collected on a JEOL JEM-ARM200CF microscope with a Cold Field Emission Gun source. Images were collected with an accelerating voltage of 200 kV. TEM samples were prepared by depositing a drop of a dilute toluene suspension of SiNPs onto a holey or ultra-thin carbon-coated copper grid (Electron Microscopy Inc.). The grid bearing the sample was kept in a vacuum chamber at a base pressure of 0.2 bar for at least 24 h prior to data collection.

Photoluminescence measurements

Photoluminescence (PL) spectra were acquired by exciting samples using the combined 352 and 364 nm lines of an argon ion laser and collecting the emission using an optical fiber interfaced to an Ocean Optics USB 2000+ Spectrometer. A 425 nm long-pass filter (LPF) was used to eliminate scattered light from the excitation source. The spectral intensity was calibrated using a blackbody radiator. Samples were prepared by dispersing the solids in toluene until the mixture was mostly clear (~2 mg mL^{-1}) and transferring ~4 mL into a 1 cm × 1 cm quartz cuvette.

Results and discussion

In this report, SiNPs of defined diameters (*i.e.*, 3 and 6 nm) were synthesized *via* thermal processing of HSQ. This well-established procedure yields silicon oxide composites containing well-defined Si(0) nano-inclusions that liberated from the oxide matrix upon ethanolic hydrofluoric acid etching.[44] The resulting hydrogen-terminated SiNPs (*i.e.*, H-SiNPs) were functionalized using sonochemically-initiated dehydrogenative coupling. Reaction products were characterized to assess the resulting surface (*i.e.*, identity and extent of functionalization), crystallinity of the SiNP core, degree of surface oxidation, and optical properties.

All H-SiNPs were orange/amber solids and exhibited poor compatibility with common organic solvents. The FT-IR spectrum of freshly etched 6 nm H-SiNPs (Fig. 1a) is representative of all nanoparticle starting materials and exhibits a prominent Si–H stretching band at 2100 cm^{-1}. We also note a comparatively weak Si–O–Si stretching feature near 1000 cm^{-1} that we attribute to minor oxidation arising from ambient exposure during sample handling. The limited solvent compatibility of H-SiNPs hindered effective sample preparation for electron microscopy and limited the utility of these methods.

As expected, H-SiNPs form opaque suspensions in toluene-based silane solutions. After sonicating for 24 h in the presence of radical initiator a notable change in the appearance of the reaction mixture is observed suggested the SiNPs had become more compatible with the organic solvent. This observation is consistent with previous dehydrocoupling-based nanoparticle functionalization (Fig. S1)[45] and can be qualitatively attributed to surface modification arising from reactions between the H-SiNPs and the silanes.[38,46–48]

In order to determine the extent of the reactivity, we first utilized FT-IR spectroscopy. For convenience we will discuss the representative results for the reaction between 6 nm H-SiNPs, AIBN and dodecylsilane sonicated for 24 h at room temperature. Similar results for 3 nm SiNPs are provided in the SI. There was no evidence supporting functionalization (*i.e.*, FT-IR, TGA, *etc.*) for short reaction times, nor for reaction mixtures that did not include a radical initiator (Fig. S3). The FT-IR spectrum (Fig. 1a) shows a sharp feature at 2900 cm^{-1} that is consistent with C–H stretching,[49,50] and the Si–H stretching feature at 2100 cm^{-1} is significantly diminished compared to the H-SiNPs that are all indicative of surface functionalization. The Si–O–Si feature at *ca.* 1000 cm^{-1} is consistent with limited oxidation arising from ambient oxidation. These spectral features, together with the change in solvent compatibility are consistent with surface grafting of the silane. Successful surface functionalization is also supported by TGA data (Fig. 1b) that provides a surface coverage of *ca.* 6% (see SI for calculation details). This degree of functionalization is consistent with other reports involving metallocene-catalyzed dehydrocoupling reactions on silicon surfaces (*e.g.*, reports of octadecylsilane and hexylsilane leading to surface coverages of 3 and 8%, respectively).[37]

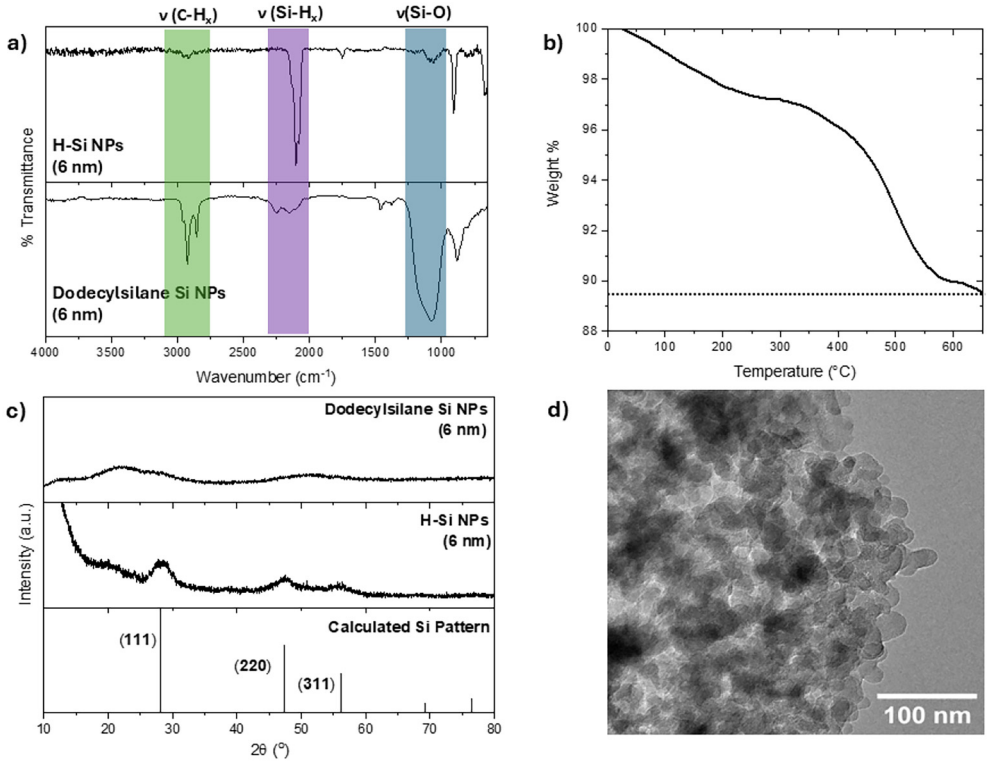

Fig. 1 (a) FT-IR spectra of H-SiNPs (top) and dodecylsilane-terminated SiNPs (bottom). (b) TGA curve of dodecylsilane-NPs (c) XRD patterns of H-SiNPs, dodecylsilane-NPs, and calculated bulk Si and (d) Bright-field TEM image of dodecylsilane-SiNPs.

Turning our focus to the physical integrity of the SiNPs, we investigated their crystallinity using powder X-ray diffraction (Fig. 1c). The patterns reveal dramatic broadening of the characteristic Si reflections after functionalization that is consistent with amorphization.[51,52] There may be many possible causes of this degradation in SiNP crystallinity. For example, an amorphous layer of silane polymer may form on the SiNP surface, SiNPs may oxidize, and/or reactions involving surface tethered silanes and the underlying core could occur. The comparatively low mass loss observed in TGA analysis precludes the possibility that a surface bonded silane-based polymer is formed, and while there is evidence for limited surface oxidation in the FTIR and XPS spectra (*vide infra*), the present observations are consistent with other functionalization methods.[46] In addition, when the dehydrogenative coupling reaction is performed under identical conditions in the absence of one reactant (*i.e.*, without silane or radical initiator), the SiNP crystallinity was preserved (Fig. S2). These observations suggest that surface tethering of a silane provides a pathway for compromising particle crystallinity. Having noted this loss of crystallinity, we sought to investigate if particle morphology was also compromised. Bright-field TEM imaging (Fig. 1d) reveals heavily agglomerated/aggregated particles consistent with the poor solution compatibility of SiNPs with limited surface functionalization. Even so, it is possible to observe clusters of intact particles and at the edges of clusters, showing that the morphology of the starting material was preserved (Fig. S4).

XPS was performed in order to confirm the composition and silicon oxidation states of the functionalized SiNPs. The survey XP spectrum (Fig. S5) confirms that the SiNPs consist of only Si, C and O with evidence of trace (*ca.* 1%) F.[53] A representative high-resolution spectrum of the Si 2p region obtained from sonication of H-SiNPs with dodecylsilane and AIBN is presented in Fig. 2a. Standard fitting of the spectral envelope based on the known silicon oxidation states reveals a large Si (0) contribution (26 atomic %, centered at 99.5 eV), with smaller components arising from Si(I) (4 atomic %, centered on 100.5 eV) and Si(III) (17 atomic %, centered on 102.5 eV), and a dominant contribution from Si(IV) (53 atomic %, centered on 103.4 eV).[54] These results are consistent with the observations and analyses discussed above, and we may conclude that the as-prepared SiNPs undergo slightly more oxidation compared to other functionalization methods (*i.e.*, hydrosilylation), consistent with the lower surface coverage.

We previously demonstrated that amorphous shells on silicon nanoparticle surfaces influence the photoluminescence.[55] Looking to the photoluminescence spectrum of silane-SiNPs prepared here (Fig. 2b), we note that small particles known to possess a disordered core show a PL maximum (λ_{max} = 610 nm) and bandwidth (140 nm) consistent with that observed for SiNPs functionalized using other methods.[46] Looking to the spectrum of the 6 nm particles that contain a core that is more ordered,[56] we find that the PL maximum (λ_{max} = 752 nm) is consistent with that observed for SiNPs

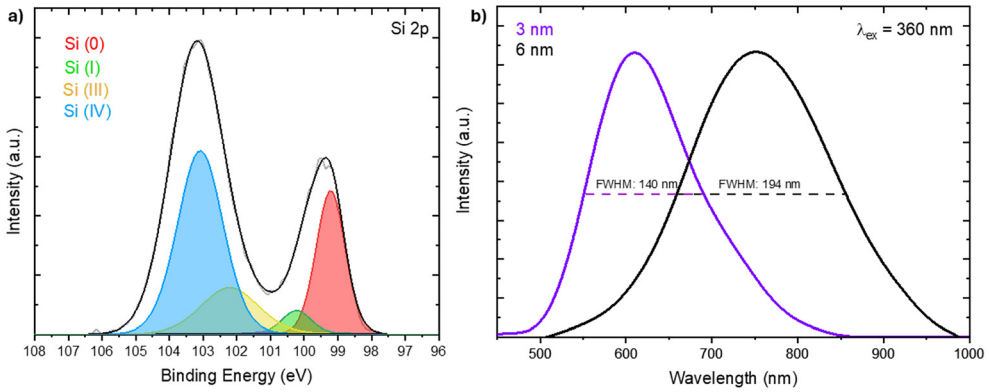

Fig. 2 (a) High Resolution Si 2p XP spectrum of 6 nm dodecylsilane SiNPs sonicated for 24 h with AIBN. Si $2p_{1/2}$ envelopes omitted for clarity. (b) Normalized photoluminescence spectra of 3 (purple) and 6 (black) nm dodecylsilane-SiNPs sonicated for 24 h with AIBN.

modified using standard hydrosilation methods, however the bandwidth is somewhat broadened (*i.e.*, 194 *vs. ca.* 175 nm), likely because of their increasingly amorphous character.[55]

Silane substitution effects

Having observed reactivity with a primary alkyl silane, we expanded the reagent scope. The substitution of the silane can have a significant impact on its reactivity – in previous studies, aryl and alkyl primary silanes led to different surface coverages (*i.e.*, 14% *vs.* 3%), with aryl silanes being much more reactive on porous silicon.[37] We elected to test the reactivity of phenylsilane here, and subjected it to the same sonochemical dehydrocoupling conditions used for dodecylsilane. The results are presented in Fig. 3. The FT-IR spectrum (3a) reveals vibrations corresponding to CH_x stretching and bending at *ca.* 2950 cm^{-1} and 1400 cm^{-1}, Si–H stretching at 2100 cm^{-1}, and Si–O–Si stretching at *ca.* 1090 cm^{-1}. These assignments are consistent with a small amount of phenylsilane amidst a partially oxidized Si–H surface; this is also supported by a surface coverage of 5%, obtained from TGA (3b). These results are comparable to those obtained for our representative alkyl silane – therefore, we conclude that the reactivities of aryl and alkyl silanes are comparable with the present sonochemical method.

The next step in examining the reagent scope was to investigate secondary and tertiary silanes, because in molecular systems these reagents are less reactive under conditions used for their primary analogues.[31] Additionally, previous dehydrocoupling studies of silanes on silicon surfaces focused only the reactivity of primary silanes.[37,39] Diisopropylsilane and trioctylsilane were the secondary and tertiary silanes of choice, respectively. They were subjected to the same reaction conditions as the primary silanes, and the results are presented in Fig. 4. FT-IR confirms that the C–H_x absorptions at 2900 cm^{-1} and 1400 cm^{-1} are present in both samples. Residual Si–H stretching is also observed at 2100 cm^{-1}, and Si–O–Si stretching at 1000 cm^{-1} is present in both samples. TGA (Fig. 4b) indicates a similar surface coverage of both silanes to that of dodecylsilane, *ca.* 8%. As in the aryl *vs.* alkyl case, we observe no significant dependence of the reaction on the silane used, as both secondary and tertiary silanes lead to similar levels of surface coverage as the primary silane does, in contrast to molecular catalyzed systems. We also observe the same loss of crystallinity in the secondary and tertiary systems, with com-

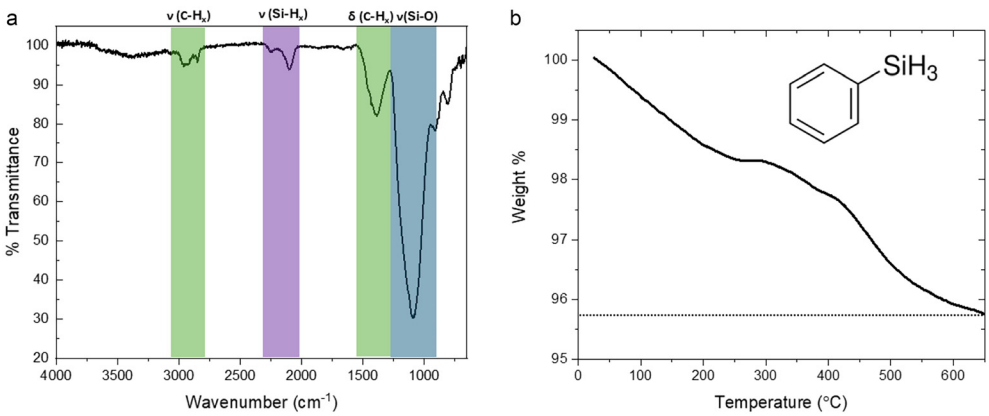

Fig. 3 (a) FT-IR spectrum and (b) TGA curve of 6 nm phenylsilane-SiNPs sonicated for 24 h in the presence of AIBN.

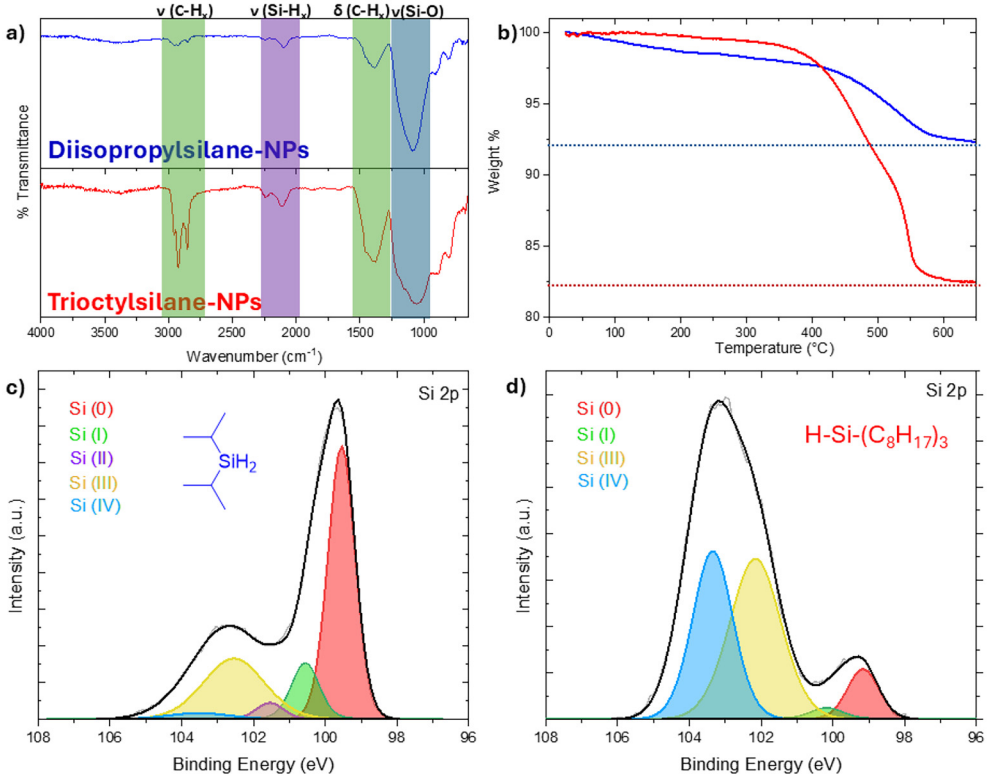

Fig. 4 (a) FT-IR Spectra and (b) TGA curves of diisopropyl- (blue) and trioctyl- (red) functionalized 6 nm SiNPs. XP Spectra of (c) diisopropyl- and (d) trioctyl-functionalized 6 nm SiNPs.

parable XRD and PL spectra presented in the SI (Fig. S6 and S7).

High-resolution Si 2p XP spectra of the secondary and tertiary silane-SiNPs are presented in Fig. 4c and d, respectively. The fitted spectral envelopes show larger proportions of Si(III) compared to the primary silane case (*i.e.*, 17 atomic %, *vide supra*). The diisopropyl-functionalized SiNPs show Si(III) at 27 atomic % (with smaller Si(IV) and Si(II) components of 3 atomic %, 11 atomic % Si(I), and 55% Si(0)), while the trioctylsilane-functionalized SiNPs show Si(III) at 49 atomic %, compared to a Si(IV) contribution of 40 atomic %. It also features a smaller Si(0) contribution of 7 atomic %. These XP spectra are consistent with partially functionalized particles that have oxidized; however, the oxidation is not the traditional Si(IV)-dominated composition arising from SiO_2.

With a variety of silanes demonstrating reactivity, it is of importance to compare the effectiveness of the present sonochemical method to other high temperature (*i.e.*, 80 °C) catalyst-free dehydrocoupling methods that have been used to modify silicon surfaces.[39] The FT-IR and TGA plots of the products resulting from heating each of dodecylsilane, diisopropylsilane, and trioctylsilane with H-SiNPs at 80 °C are presented in Fig. 5. The thermal reaction involving dodecylsilane results in a similar degree of functionalization to the present sonochemical case, with a *ca.* 8% surface coverage and the expected peaks in the FT-IR spectrum (*i.e.*, C–H_x, Si–H, Si–O–Si). The other two silanes, conversely, show no C–H_x stretching peaks in the FT-IR spectra, and TGA indicates negligible mass loss, leading us to conclude that no functionalization took place. In addition, the XRD spectra (Fig. S8) show that both the dodecylsilane-SiNPs and the diisopropylsilane-SiNPs maintain their crystallinity, in contrast to the sonochemical samples. Thus, the sonochemical reaction leads to functionalization with substituted silanes where the thermal reaction does not, and leads to comparable coverage in the case of primary silanes. Furthermore, it allows for the formation of amorphous SiNPs, in contrast with nanoparticles prepared by the thermal reaction.

In order to explain the reactivity of the secondary and tertiary silanes, we consider the reaction mechanism, and possible differences from the thermal method. The sonochemical reaction requires a radical initiator to proceed over the timeframes studied, and thus the mechanism must involve radical activation. Ultrasonication alone does provide radicals resulting from surface bond breakage; the need for a radical initiator suggests sonication alone leads to an insufficient radical concentration to activate silanes. The addition of a radical initiator can meet the threshold for reaction by providing more radicals, activated under sonication conditions. The thermally activated method, in contrast, proceeds at elevated temperature without a radical initiator, and the addition of a radical initiator does not provide any benefit, with 24 h still being required to achieve substantive functionalization.

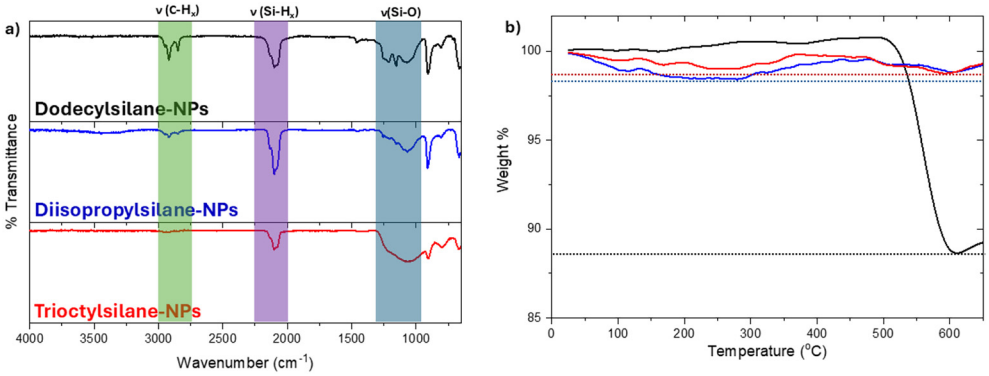

Fig. 5 (a) FT-IR spectra and (b) TGA curves of dodecyl- (black), diisopropyl- (blue), and trioctyl- (red) functionalized 6 nm SiNPs treated at 80 °C.

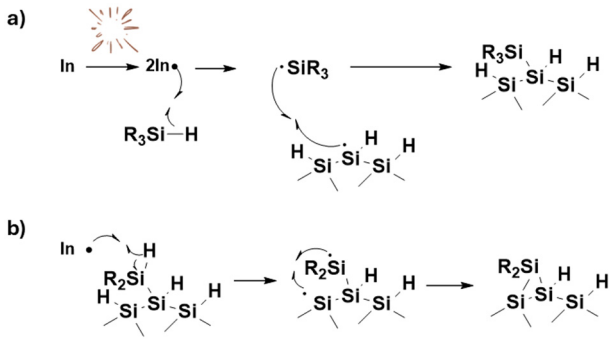

Fig. 6 (a) Radically-initiated sonochemical dehydrocoupling of silanes and (b) Propagation with secondary and/or primary silanes to form multiple Si–Si bonds on the surface. Cavitation bubble-induced bond breakage is omitted for clarity, but may replace the role of the initiator in any of the events shown.

We propose that the sonochemical reaction presented here proceeds *via* the mechanism shown in Fig. 6.[46] Surface Si–H/Si–Si and silane Si–H bonds are broken by cavitation bubble collapse or radical initiator involvement, and the resulting radicals react forming Si–Si bonds linking silanes to the particle surface (Fig. 6a). The Si–H bonds on the surface bonded silane can then undergo further cleavage to form radicals that propagate (if the silane is secondary or primary) leading to different surface linkages (Fig. 6b). This propagation is terminated if there are no accessible neighbouring Si–H sites. This mechanism and the associated surface bonding provide an explanation for the reduced surface coverage provided by dehydrocoupled silanes compared to hydrosilylated alkenes – surface reactions with primary silanes can consume up to three Si–H surface sites, while more substituted silanes prevent surface reactions because of their steric bulk.

This mechanistic understanding is consistent with reactivity of 'over-etched' SiNPs.[56] For 6 and 9 nm particles, over-etching removes the disordered surface to expose the quasi-ordered core, which will have fewer defects and Si–H$_x$ reactive sites. One would anticipate this surface would exhibit a lower reactivity if the proposed mechanism is accurate. Sonochemical dehydrocoupling reactions using dodecylsilane with over-etched 6 nm SiNPs (final diameter 3 nm) were consistent with this hypothesis, leading to a surface coverage of 2% (Fig. S11), lower than that of the traditionally etched particles (5%).

To explore the effect of different radical sources, and to support that the reactivity is in fact radical based, the sonochemical dehydrocoupling was run with benzoyl peroxide,

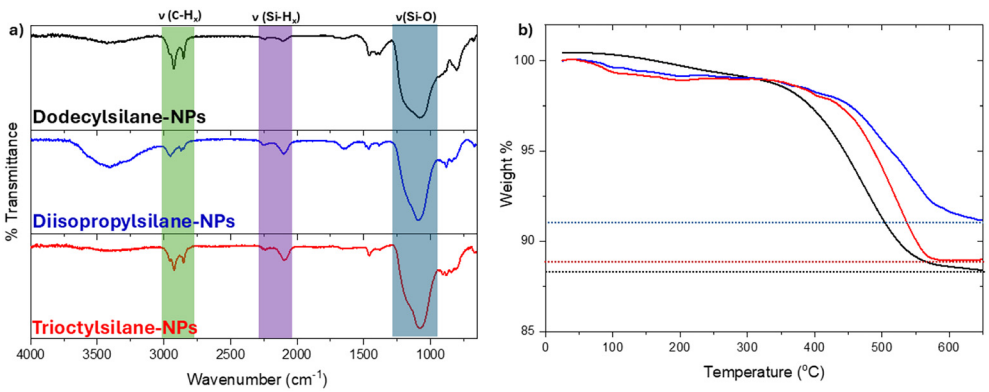

Fig. 7 (a) FT-IR spectra and (b) TGA curves of dodecyl- (black), diisopropyl- (blue), and trioctyl- (red) functionalized 6 nm SiNPs sonicated for 24 h in the presence of benzoyl peroxide.

another common radical initiator with similar reactivity to AIBN. Comparable reactivity is observed to AIBN, with no significant differences in the FT-IR and a surface coverage of 8% obtained from TGA (Fig. 7).

Conclusions

Successful dehydrocoupling has been demonstrated at room temperature using ultrasonication to functionalize hydride-terminated silicon nanoparticles. FT-IR and TGA were used to confirm that comparable reactivity to previous examples of dehydrocoupling on silicon surfaces was achieved with primary silanes (both alkyl and aryl), with *ca.* 7% surface coverage. Surprisingly, the functionalized particles exhibit a loss of crystallinity, providing a straightforward pathway to amorphous SiNPs which maintain their photoluminescence. In addition, secondary and tertiary silanes were grafted using this method, which has not been previously reported without catalytic intervention, and these silanes led to comparable surface coverages as for the primary silanes. These substituted silanes were also shown to react under photo-initiated conditions at room temperature. A radical-based mechanism is proposed to be responsible for this reactivity, similar to that of radically initiated hydrosilylation. This approach can lead to a wider variety of silanes being grafted to the silicon surface, as well as providing an amorphous SiNP base for further chemistry.

Conflicts of interest

There are no conflicts of interest to declare.

Data availability

The data supporting the findings of this report have been included in the article and the supplementary information (SI), with raw data available upon request of the corresponding author.

Supplementary information is available. See DOI: https://doi.org/10.1039/d5nr04768d.

Acknowledgements

We thank the Analytical lab services at the University of Alberta for assistance in collecting FTIR data. We thank the UofA nanoFAB facility for access to XPS and electron microscopy facilities. Additionally, we recognize the continued generous funding from the Natural Science and Engineering Research Council (NSERC Discovery Grant program; RGPIN-2020-04045), Alberta Innovates, the ATUMS training program supported by NSERC CREATE (CREATE-463990-2015) as well as the University of Alberta Faculties of Science and Graduate Studies.

References

1 M. Di Sabatino, R. Hendawi and A. S. Garcia, *Crystals*, 2024, **14**(2), 167–182.
2 S. Shekhar, W. Bogaerts, L. Chrostowski, J. E. Bowers, M. Hochberg, R. Soref, *et al.*, *Nat. Commun.*, 2024, **15**(1), 751–766.
3 H. L. Ye, Y. Shang, H. Y. Wang, Y. L. Ma, X. W. He, W. Y. Li, *et al.*, *Talanta*, 2021, **230**, 122294–122304.
4 A. Jana, S. Cho, A. Meena, A. T. A. Ahmed, V. G. Sree, Y. Park, *et al.*, *InfoMat*, 2024, **6**(12), e12559.
5 J. Sobhanan, J. V. Rival, A. Anas, E. Sidharth Shibu, Y. Takano and V. Biju, *Adv. Drug Delivery Rev.*, 2023, **197**, 114830–114865.
6 Y.-J. Wu, Y.-A. Chen, C.-L. Huang, J.-T. Su, C.-T. Hsieh and S.-Y. Lu, *Chem. Eng. J.*, 2020, **400**, 125958–125969.
7 A. Boretti and S. Castelletto, *Silicon*, 2025, **17**(8), 1799–1810.
8 J. K. Lee, C. Oh, N. Kim, J.-Y. Hwang and Y.-K. Sun, *J. Mater. Chem. A*, 2016, **4**(15), 5366–5384.
9 L. Mahawar, K. P. Ramasamy, M. Suhel, S. M. Prasad, M. Zivcak, M. Brestic, *et al.*, *Environ. Res.*, 2023, **232**, 116292–116306.
10 C. F. Wang, E. M. Makila, M. H. Kaasalainen, M. V. Hagstrom, J. J. Salonen, J. T. Hirvonen, *et al.*, *Acta Biomater.*, 2015, **16**, 206–214.
11 V. S. Shankar, G. Velmurugan, D. E. Raja, T. Manikandan, S. S. Kumar, J. Singh, *et al.*, *Silicon*, 2023, **16**(3), 979–988.
12 L. Nayak, S. Mohanty, S. K. Nayak and A. Ramadoss, *J. Mater. Chem. C*, 2019, **7**(29), 8771–8795.
13 S. H. Ko, *Semicond. Sci. Technol.*, 2016, **31**(7), 073003–073026.
14 N. Kannan and N. Gupta, *IEEE J. Flex. Electron.*, 2024, **3**(10), 436–444.
15 B. P. Falcao, J. P. Leitao, L. Ricardo, H. Aguas, R. Martins and R. N. Pereira, *Appl. Mater. Today*, 2021, **23**, 101071–101081.
16 R. J. Clark, M. K. Dang and J. G. C. Veinot, *Langmuir*, 2010, **26**, 15657–15664.
17 M. Dasog, G. B. De los Reyes, L. V. Titova, F. A. Hegmann and J. G. C. Veinot, *ACS Nano*, 2014, **8**, 9636–9648.
18 J. P. Bell, J. E. Cloud, J. Cheng, C. Ngo, S. Kodambaka, A. Sellinger, S. K. R. Williams and Y. Yang, *RSC Adv.*, 2014, **4**, 51105–51110.
19 J. M. Buriak, *Chem. Commun.*, 1999, **12**, 1051–1060.
20 T. K. Purkait, M. Iqbal, M. A. Islam, M. H. Mobarok, C. M. Gonzalez, L. Hadidi and J. G. C. Veinot, *J. Am. Chem. Soc.*, 2016, **138**, 7114–7120M.
21 R. Linford and C. E. D. Chidsey, *J. Am. Chem. Soc.*, 1993, **115**, 12631–12632.
22 M. R. Linford, P. Fenter, P. M. Eisenberger and C. E. D. Chidsey, *J. Am. Chem. Soc.*, 1995, **117**, 3145–3155.
23 J. Terry, R. Mo, C. Wigren, R. Cao, G. Mount, P. Pianetta, M. R. Linford and C. E. D. Chidsey, *Nucl. Instrum. Methods Phys. Res., Sect. B*, 1997, **133**(1–4), 94–101.

24 M. P. Stewart and J. M. Buriak, *Angew. Chem., Int. Ed.*, 1998, **37**(23), 3257–3260.
25 J. M. Buriak and M. J. Allen, *J. Am. Chem. Soc.*, 1998, **120**, 1339–1340.
26 M. H. Mobarok, T. K. Purkait, M. A. Islam, M. Miskolzie and J. G. C. Veinot, *Angew. Chem., Int. Ed.*, 2017, **56**, 6073–6077.
27 A. Bansal, X. Li, I. Lauermann, N. S. Lewis, S. I. Yi and W. H. Weinberg, *J. Am. Chem. Soc.*, 1996, **118**(30), 7225–7226.
28 J. H. Warner, A. Hoshino, K. Yamamoto and R. D. Tilley, *Angew. Chem., Int. Ed.*, 2005, **44**, 4550.
29 J. F. Brown, L. H. Vogt, A. Katchman, J. W. Eustance, K. M. Kiser and K. W. Krantz, *J. Am. Chem. Soc.*, 1960, **82**(23), 6194–6195.
30 L. H. Sommer and J. D. Citron, *J. Org. Chem.*, 1967, **32**, 2470–2472.
31 S. J. Rettig, *Inorg. Chim. Acta*, 1994, **222**, 345–364.
32 I. Ojima, T. Kogure and S.-I. Inaba, *J. Organomet. Chem.*, 1973, **55**, C7–C8.
33 C. Aitken, J. F. Harrod and E. Samuel, *J. Organomet. Chem.*, 1985, **279**, C11–C13.
34 J. Y. Corey, X.-H. Zhu, T. C. Bedard and L. D. Lange, *Organometallics*, 1991, **10**, 924–930.
35 S. Azpeitia, B. Fernández, M. A. Garralda and M. A. Huertos, *Eur. J. Inorg. Chem.*, 2016, **18**, 2891–2895.
36 M. Itazaki, K. Ueda and H. Nakazawa, *Angew. Chem., Int. Ed.*, 2009, **48**(18), 3313–3316.
37 J. Buriak, *Inorg. Chem.*, 2006, **45**, 1096–1102.
38 Z. Yang, M. H. Wahl and J. G. C. Veinot, *Can. J. Chem.*, 2014, **92**(10), 951–957.
39 D. Kim, J. Joo, Y. Pan, A. Boarino, Y. W. Jun, K. H. Ahn, *et al.*, *Angew. Chem., Int. Ed.*, 2016, **55**(22), 6423–6427.
40 K. S. Suslick, *Science*, 1990, **247**, 1439.
41 J. H. Bang and K. S. Suslick, *Adv. Mater.*, 2010, **22**, 1039–1059.
42 R. F. Martinez, G. Cravatto and P. Cintas, *J. Org. Chem.*, 2021, 13833–13856.
43 C. M. Hessel, E. J. Henderson and J. G. C. Veinot, *Chem. Mater.*, 2006, **18**, 6139–6146.
44 J. K. Kang and C. B. Musgrave, *J. Chem. Phys.*, 2002, **116**, 275–280.
45 M. A. Hossain, M. Javadi, H. Yu, A. N. Thiessen, N. Ikpo, A. O. Oliynyk and J. G. C. Veinot, *Nanoscale*, 2020, **12**, 6271–6278.
46 J. Trach, S. Williams, B. Michalczyk, C. Butler, A. Meldrum, J. Washington and J. G. C. Veinot, *Nanoscale Adv.*, 2025, (7), 3018–3027.
47 H. Yu, A. N. Thiessen, M. A. Hossain, M. J. Kloberg, B. Rieger and J. G. C. Veinot, *Chem. Mater.*, 2020, **32**(11), 4536–4543.
48 J. Kehrle, S. Kaiser, P. K. Purkait, M. Winnacker, T. Helbich, S. Vagin, J. G. C. Veinot and B. Rieger, *Nanoscale*, 2017, **9**, 8489–8495.
49 W. L. Lin, H. K. Tsai, S. C. Lee, W. J. Sah and W. J. Tzeng, *Appl. Phys. Lett.*, 1987, **51**, 2112–2114.
50 J. H. Chen, W. J. Sah and S. C. Lee, *J. Appl. Phys.*, 1991, **70**, 125–130.
51 R. Gauthier, B. Scott, J. C. Bennet, M. Salehabadi, J. Wang, T. Sainuddin and M. N. Obrovac, *Heliyon*, 2024, **10**(15), e34881.
52 G. Zhang, Y. Xu, D. Xu, D. Wang, Y. Xue and W. Su, *High Pressure Res.*, 2008, **28**, 641–650.
53 B. Glockzin, K. O'Conner, C. Ni, C. Butler, J. G. C. Veinot and V. K. Michealis, *ACS Nano*, 2024, **18**(38), 26419–26434.
54 R. Alfonsetti, L. Lozzi, M. Passacantando, P. Picozzi and S. Santucci, *Appl. Surf. Sci.*, 1993, **70**, 222–225.
55 I. T. Cheong, L. Y. Szepesvari, C. Ni, C. Butler, K. M. O'Conner, R. Hooper, A. Meldrum and J. G. C. Veinot, *Nanoscale*, 2024, **16**, 592–603.
56 A. N. Thiessen, M. Ha, R. W. Hooper, H. Yu, A. O. Oliynyk, J. G. C. Veinot and V. K. Michaelis, *Chem. Mater.*, 2019, **31**(3), 678–688.